Heat and momentum transfer for magnetoconvection in a vertical external magnetic field

Till Zürner,* Wenjun Liu, Dmitry Krasnov, and Jörg Schumacher
Institut für Thermo- und Fluiddynamik, Technische Universität Ilmenau, Postfach 100565, D-98684 Ilmenau, Germany
(Received 1 July 2016; published 17 October 2016)

The scaling theory of Grossmann and Lohse [J. Fluid Mech. **407**, 27 (2000)] for turbulent heat and momentum transfer is extended to the magnetoconvection case in the presence of a (strong) vertical magnetic field. A comparison with existing laboratory experiments and direct numerical simulations in the quasistatic limit allows us to restrict the parameter space to very low Prandtl and magnetic Prandtl numbers and thus to reduce the number of unknown parameters in the model. Also included is the Chandrasekhar limit, for which the outer magnetic induction field $\boldsymbol{B}$ is large enough such that convective motion is suppressed and heat is transported by diffusion. Our theory identifies four distinct regimes of magnetoconvection that are distinguished by the strength of the outer magnetic field and the level of turbulence in the flow, respectively.

DOI: 10.1103/PhysRevE.94.043108

I. INTRODUCTION

One of the central questions in turbulent convection is that of the global transport of heat and momentum as a function of thermal driving and the properties of a working fluid [1–3]. In the simplest setting of turbulent convection—the Rayleigh-Bénard case—one considers an infinitely extended horizontal layer of fluid that is uniformly heated from below and cooled from above. The thermal driving of the turbulent convection in the layer is then established by the temperature difference between the top and the bottom, $\Delta T = T_{\mathrm{bottom}} - T_{\mathrm{top}}$, and is directly proportional to the dimensionless Rayleigh number Ra. The properties of the working fluid are determined by the Prandtl number Pr, defined as the ratio of the kinematic viscosity ν to the thermal diffusivity κ. Turbulent heat and momentum transfer are quantified by the dimensionless Nusselt number, Nu, and Reynolds number, Re, respectively. In a nutshell, one seeks Nu and Re as functions of Ra and Pr.

One of the oldest scaling theories that was aimed at predicting Nu(Ra) at fixed Pr dates back to Malkus [4,5], and it is based on a marginal stability argument for the turbulent mean profiles. More recently, scaling theories by Shraiman and Siggia [6,7] and Grossmann and Lohse (GL) [8,9] have been developed. The central idea of the GL theory is a decomposition of the thermal and kinetic energy dissipation into contributions from the bulk and the boundary layers in the vicinity of the plates. These contributions have to be weighted with the volume fractions that are occupied by the boundary layers of the temperature and velocity fields. The theory is adapted to doubly diffusive convection [10] and horizontal convection [11].

In astrophysical systems, thermal convection is often tightly coupled to magnetic fields (and rotation), which is known as magnetoconvection [12]. Examples are sunspots in the solar chromosphere [13] or the x-ray flaring activity of some young neutron stars, which are termed magnetars [14]. Less spectacular, but not less important, are numerous industrial applications ranging from materials processing, such as crystal growth by the Czochralski method [15] or dendritic solidification in alloys [16], to fusion technology [17]. In the case of a strong prescribed magnetic induction $\boldsymbol{B}_0$, the secondary magnetic induction $\boldsymbol{b}$, which is generated by flow-induced eddy currents, remains very small. While a strong vertical external field can then damp and even suppress the convective fluid motion [18], convection rolls can be stabilized when the magnetic field is applied in the horizontal direction [19]. From a standard magnetohydrodynamic (MHD) perspective, the turbulence of coupled velocity and magnetic fields is then constrained. This regime is known as the quasistatic regime of MHD: the Lorentz force enters the momentum equation, while the induction equation, which describes the temporal evolution of the magnetic induction field $\boldsymbol{b}$, is neglected [20].

The aim of the present work is to extend the GL theory of turbulent transport to the case of magnetoconvection. Initial attempts in this direction have been reported by Chakraborty [21]. He showed that an Ohmic dissipation rate, ε_B, has to be incorporated beside the thermal and kinetic energy dissipation rates, ε_T and ε. One is thus left with eight different regimes of boundary-layer- and/or bulk-dominated dissipation rates. Together with free parameters for the viscous boundary-layer thickness and a critical Reynolds number for the crossover from low to high Prandtl numbers [9], one ends up with at least ten parameters to fit. Furthermore, dimensionless parameters have to be added that relate the electrical conductivity σ either to the kinematic viscosity or the thermal diffusivity and quantify the strength of the outer magnetic field. In view of this significant extension of the parameter space, one has to seek regimes of magnetoconvection that can be studied with a reduced set of fit parameters.

We will therefore restrict the turbulent magnetoconvection to a specific parameter range. In view of a comparison with laboratory experiments of magnetoconvection, which are typically conducted in liquid metals, one can restrict the Prandtl number range to

$$\mathrm{Pr} = \frac{\nu}{\kappa} \lesssim 10^{-2}. \tag{1}$$

Also, the range of the magnetic Prandtl number Pm can be limited to

$$\mathrm{Pm} = \frac{\nu}{\eta} = \frac{\mathrm{Rm}}{\mathrm{Re}} \lesssim 10^{-5} \tag{2}$$

*till.zuerner@tu-ilmenau.de

with the diffusivity of the magnetic induction $\eta = 1/(\mu\sigma)$, and μ being the permeability. In many laboratory flows, the magnetic Reynolds number Rm will thus remain small, $\mathrm{Rm} \ll 1$. This regime is termed the *quasistatic* case of magnetohydrodynamics. The magnetic field lines cannot be bent significantly by the fluid motion since the magnetic diffusion time scale is very short. This excludes some astrophysical applications such as interstellar turbulent gases in which $\mathrm{Pm} \gg 1$ [22].

Similar to standard GL theory, our predictions have to be fitted to one reference dataset. Our adjustment of the free coefficients will be based on an experiment by Cioni *et al.* [23], which, to the best of our knowledge, is the only experiment that was operated at a sufficiently high Rayleigh number. Further data records by Burr and Müller [24] and Aurnou and Olson [25] have been conducted at smaller Rayleigh numbers and will be discussed only briefly. In addition, our own direct numerical simulations of magnetoconvection in the quasistatic regime will be included to obtain (at least one) data point with known Reynolds and Nusselt numbers at given Rayleigh, Hartmann (the dimensionless measure for magnetic-field strength, which will be defined in Sec. II), and Prandtl numbers.

The outline of the work is as follows. In the next section, the set of magnetoconvective equations of motion is discussed, and the characteristic scales, dimensionless parameters, and dissipation rates are defined. In addition, the numerical method and a short description of the datasets will be presented. This section is followed by a derivation of the nonlinear equations for Nu and Re. Finally, the free parameters of the scaling theory are fitted to data records. The results are summarized and discussed briefly at the end of the work.

II. EQUATIONS AND PARAMETERS

A. Quasistatic equations of magnetoconvection in Boussinesq approximation

We solve the three-dimensional Boussinesq equations for turbulent magnetoconvection in a rectangular cell of height H and side lengths L in the quasistatic limit. The equations for the velocity field $\boldsymbol{u}(\boldsymbol{x},t)$ and the temperature field $T(\boldsymbol{x},t)$ are given by

$$\nabla \cdot \boldsymbol{u} = 0, \tag{3}$$

$$\frac{\partial \boldsymbol{u}}{\partial t} + (\boldsymbol{u}\cdot\nabla)\boldsymbol{u} = -\frac{1}{\rho_0}\nabla p + \nu\nabla^2\boldsymbol{u} + g\alpha(T - T_0)\boldsymbol{e}_z + \frac{1}{\rho_0}(\boldsymbol{j}\times\boldsymbol{B}_0), \tag{4}$$

$$\frac{\partial T}{\partial t} + (\boldsymbol{u}\cdot\nabla)T = \kappa\nabla^2 T. \tag{5}$$

The pressure field is denoted $p(\boldsymbol{x},t)$, T_0 is a reference temperature, ρ_0 is the constant mass density, and $\boldsymbol{B}_0 = B_0\boldsymbol{e}_z$ is the magnetic field. The Ohm law for the current density is given by

$$\boldsymbol{j} = \sigma(-\nabla\phi + \boldsymbol{u}\times\boldsymbol{B}_0), \tag{6}$$

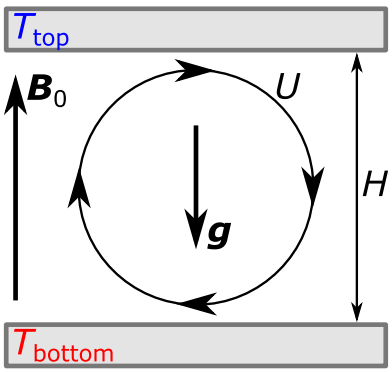

FIG. 1. Magnetoconvection flow. The outer magnetic induction $\boldsymbol{B}_0 = B_0\boldsymbol{e}_z$, the acceleration due to gravity $\boldsymbol{g} = (0,0,-g)$, the temperature difference, and the characteristic large-scale velocity are indicated.

where the electric potential ϕ follows from $\nabla\cdot\boldsymbol{j} = 0$. The Rayleigh number is given by

$$\mathrm{Ra} = \frac{g\alpha\Delta T H^3}{\nu\kappa}, \tag{7}$$

and the Hartmann number by

$$\mathrm{Ha} = B_0 H\sqrt{\frac{\sigma}{\rho_0\nu}} = \sqrt{Q}. \tag{8}$$

The square of Ha is also known as the Chandrasekhar number Q. The variables g, σ, and α denote the acceleration due to gravity, the electrical conductivity, and the thermal expansion coefficient, respectively. In a dimensionless form, length scales are expressed in units of H, velocities in units of the free-fall velocity $U_f = \sqrt{g\alpha\Delta T H}$, temperature in units of the outer difference ΔT, and magnetic induction in units of B_0. The configuration is sketched in Fig. 1.

B. Direct numerical simulations

Equations (3)–(6) are solved for a closed Cartesian cell with a second-order finite-difference scheme. The projection-type scheme is nearly fully conservative. The advection-diffusion equation is solved by semi-implicit scheme in which nonlinear terms are treated explicitly and diffusion terms implicitly. The program applies MPI and Open MP. More details are found in [26]. For the fit, we will use two series of direct numerical simulations (DNS):

Series 1: $\mathrm{Ra} = 10^5$,$\mathrm{Pr} = 0.025$,$20 \leqslant \mathrm{Ha} \leqslant 50$. The aspect ratios are $\Gamma_x = L_x/H = 1$ and $\Gamma_y = L_y/H = 1$. The grid is nonuniform and contains 128^3 points.

Series 2: $\mathrm{Ra} = 10^6$,$\mathrm{Pr} = 0.025$,$50 \leqslant \mathrm{Ha} \leqslant 200$. The aspect ratios are $\Gamma_x = L_x/H = 1$ and $\Gamma_y = L_y/H = 1$. The grid is nonuniform and contains 128^3 points.

The boundary conditions are as follows: all walls are electrically insulated walls, i.e., the electric current forms closed loops inside the fluid volume. No-slip boundary conditions hold for the velocity at all walls. The top and bottom walls are isothermal with prescribed temperatures T_{top} and $T_{\mathrm{bottom}} > T_{\mathrm{top}}$, respectively, the side walls are thermally insulated ($\partial T/\partial n = 0$). The grid is clustered at the top and bottom walls to resolve the Hartmann layers and first-order

quantities. We have also performed grid-sensitivity studies to make sure that the Nusselt number remains constant plane-by-plane (plane at constant height z).

C. Dissipation rate balances

In correspondence with classical Rayleigh-Bénard convection, we can derive exact relations for the mean kinetic energy dissipation rate, ε, the mean magnetic dissipation rate, ε_B, and the mean thermal dissipation rate, ε_T. The fields are defined as

$$\varepsilon(\boldsymbol{x},t) = \frac{\nu}{2}(\partial_i u_j + \partial_j u_i)^2, \tag{9}$$

$$\varepsilon_B(\boldsymbol{x},t) = \frac{\eta}{2\mu\rho_0}(\partial_i b_j - \partial_j b_i)^2, \tag{10}$$

$$\varepsilon_T(\boldsymbol{x},t) = \kappa(\partial_i T)^2, \tag{11}$$

with $i,j = x,y,z$. Since $\boldsymbol{B}_0$ is constant, Eq. (10) contains derivatives of the induced magnetic induction $\boldsymbol{b}$ only, which arises from the eddy currents $\boldsymbol{j}$. In the statistically stationary regime, we obtain

$$\varepsilon + \varepsilon_B = \frac{\nu^3}{H^4}\frac{(\mathrm{Nu}-1)\mathrm{Ra}}{\mathrm{Pr}^2}, \tag{12}$$

$$\varepsilon_T = \kappa\frac{(\Delta T)^2}{H^2}\mathrm{Nu}. \tag{13}$$

The Nusselt number, which quantifies the turbulent heat transfer, is given by

$$\mathrm{Nu} = 1 + \frac{H\langle u_z T\rangle}{\kappa\Delta T}. \tag{14}$$

The global momentum transfer in the magnetoconvective system is quantified by the Reynolds number, which is defined as

$$\mathrm{Re} = \frac{\langle u_i^2\rangle^{1/2} H}{\nu}. \tag{15}$$

In both definitions, $\langle\cdot\rangle$ stands for volume-time average or ensemble average. While the thermal balance remains unchanged in comparison to the classical Rayleigh-Bénard case, the kinetic energy balance differs by the addition of ε_B on the left-hand side of Eq. (12). It results from the Joule dissipation in the presence of a magnetic field. For completeness, we also list the definition of the magnetic Reynolds number,

$$\mathrm{Rm} = \frac{UH}{\eta} = \mu\sigma UH, \tag{16}$$

where U is again given by the root-mean-square velocity, $U = \langle u_i^2\rangle^{1/2}$.

III. EXTENSION OF THE SCALING THEORY OF GROSSMANN AND LOHSE

The central idea of the scaling theory is to combine Eqs. (12) and (13) with a decomposition of dissipation rates into contributions coming from the bulk and the boundary layers (BL) [8,9]. The following modifications are made to predict Nu(Ra, Pr, Ha) and Re(Ra, Pr, Ha) for our case at hand:

(i) The relevant boundary layer for the velocity field is the Hartmann layer [20] (see also the Appendix),

$$\delta_v = \frac{H}{\mathrm{Ha}}, \tag{17}$$

while the thermal boundary-layer thickness remains $\delta_T = H/(2\,\mathrm{Nu})$. Contrary to the original GL theory, we do not have the free parameter a that appears in the Prandtl-Blasius-type expression, $\delta_v = aH/\sqrt{\mathrm{Re}}$.

(ii) We limit the study to low Prandtl numbers as already mentioned in the Introduction. Thus the modification for the limit of large Prandtl numbers, which has been developed in [9], and the related parameter Re_c are not necessary here. This saves a second fit parameter.

(iii) It is well known from the linear stability analysis [18] that the critical Rayleigh number Ra_c scales as

$$\mathrm{Ra}_c = \pi^2\mathrm{Ha}^2. \tag{18}$$

If Ha is too big at a given Ra, convection is suppressed completely.

The mean energy dissipation rates will be composed of a boundary-layer contribution and a bulk contribution. This results in

$$\varepsilon = \varepsilon_{\mathrm{bulk}} + \varepsilon_{\mathrm{BL}}, \tag{19}$$

$$\varepsilon_B = \varepsilon_{B,\mathrm{bulk}} + \varepsilon_{B,\mathrm{BL}}, \tag{20}$$

$$\varepsilon_T = \varepsilon_{T,\mathrm{bulk}} + \varepsilon_{T,\mathrm{BL}}. \tag{21}$$

The dimensional estimates of the different contributions are given by

$$\varepsilon_{\mathrm{bulk}} \sim \frac{U^3}{H} = \frac{\nu^3}{H^4}\mathrm{Re}^3, \tag{22}$$

$$\varepsilon_{\mathrm{BL}} \sim \nu\frac{U^2}{\delta_v^2}\frac{\delta_v}{H} = \frac{\nu^3}{H^4}\mathrm{Re}^2\mathrm{Ha}, \tag{23}$$

$$\varepsilon_{B,\mathrm{bulk}} \sim \frac{\eta}{\mu\rho_0}\frac{\mathrm{Rm}^2 B_0^2}{H^2} = \frac{\nu^3}{H^4}\mathrm{Re}^2\mathrm{Ha}^2, \tag{24}$$

$$\varepsilon_{B,\mathrm{BL}} \sim \frac{\eta}{\mu\rho_0}\frac{\mathrm{Rm}^2 B_0^2}{\delta_v^2}\frac{\delta_v}{H} = \frac{\nu^3}{H^4}\mathrm{Re}^2\mathrm{Ha}^3, \tag{25}$$

$$\varepsilon_{T,\mathrm{bulk}} \sim \frac{(\Delta T)^2 U}{H} = \kappa\frac{(\Delta T)^2}{H^2}\mathrm{Re}\,\mathrm{Pr}, \tag{26}$$

$$\varepsilon_{T,\mathrm{BL}} \sim \kappa\frac{(\Delta T)^2}{H^2}\sqrt{\mathrm{Re}\,\mathrm{Pr}}\,. \tag{27}$$

The bulk scalings of the kinetic and thermal dissipation rates in (22) and (26) are the same as in the original GL theory [9]. The argumentation in [9] that leads to (27) remains valid for the present case. However, the scaling relation in (23) differs from the original case. Instead of the original BL expression $\delta_v^{\mathrm{GL}} = aL/\sqrt{\mathrm{Re}}$, we insert the Hartmann layer thickness (17). For the new estimates in (24) and (25) we use the definition of ε_B, which is given in (10), and we measure the induced magnetic field $\boldsymbol{b}$ in units of $\mathrm{Rm}B_0$.

Following Grossmann and Lohse [9], we introduce interpolation functions to account for changes of the scaling laws in different parameter regimes. Once δ_T becomes smaller than δ_v, the dominant velocity in the thermal BL changes from U to

$U\delta_T/\delta_v$. This is accounted for by replacing Re with $\mathrm{Re}\, f(x_T)$ in (26) and (27), where

$$f(x_T) = \frac{1}{\left(1 + x_T^n\right)^{1/n}} \tag{28}$$

with the argument $x_T = \delta_v/\delta_T = 2\,\mathrm{Nu}/\mathrm{Ha}$ and $n = 4$. For this interpolation function, it follows that $f(x_T \to 0) \to 1$ and $f(x_T \to \infty) \to 1/x_T$.

Close to the critical Rayleigh number, the bulk of the fluid becomes laminar and $\varepsilon_{\mathrm{bulk}}$ scales with Re^2 rather than Re^3 as in (22) for the turbulent regime. This change is modeled by multiplying (22) with

$$g(x^*) = \frac{1}{f(1/x^*)} \tag{29}$$

with the argument $x^* = \mathrm{Re}/\mathrm{Re}^*$. From the definition of f, it follows that $g(x^* \to 0) \to 1/x^*$ and $g(x^* \to \infty) \to 1$. The Reynolds number Re^* marks the range in which the transition from fully developed turbulence to the weakly nonlinear time-dependent regime of velocity dynamics takes place. Combining all pure scaling laws with the interpolations as just described gives

$$\frac{(\mathrm{Nu}-1)\mathrm{Ra}}{\mathrm{Pr}^2\mathrm{Re}^2} = c_1 \mathrm{Re}\, g\left(\frac{\mathrm{Re}}{\mathrm{Re}^*}\right) + c_2\mathrm{Ha} + c_3\mathrm{Ha}^2 + c_4\mathrm{Ha}^3, \tag{30}$$

$$\mathrm{Nu} - 1 = c_5 \mathrm{Re}\,\mathrm{Pr} f\left(\frac{2\,\mathrm{Nu}}{\mathrm{Ha}}\right) + c_6\sqrt{\mathrm{Re}\,\mathrm{Pr} f\left(\frac{2\,\mathrm{Nu}}{\mathrm{Ha}}\right)}, \tag{31}$$

with the seven *a priori* unknown model parameters Re^* and c_1–c_6, which have to be determined from a data record. The set of implicit equations can then be solved to obtain expressions Nu(Ra,Ha,Pr) and Re(Ra,Ha,Pr). While it is not possible to find a full solution analytically, Re can be calculated from (31) as a function of Nu, Ra, Ha, and Pr:

$$\mathrm{Re} = \frac{\left(\sqrt{c_6^2 + 4c_5(\mathrm{Nu}-1)} - c_6\right)^2}{4c_5^2 \mathrm{Pr} f\left(\frac{2\,\mathrm{Nu}}{\mathrm{Ha}}\right)}. \tag{32}$$

Inserting (32) into (30) gives an equation independent of Re. However, this new equation cannot be solved analytically for Nu.

The stabilizing effect (iii) of large Ha is included here in the following way: assuming we have found an analytical expression $\mathrm{Nu} - 1 = \mathcal{N}(\mathrm{Ha},\mathrm{Ra},\mathrm{Pr})$, we can enforce the transition to the nonconvective regime at $\mathrm{Ra} = \mathrm{Ra}_c$ by multiplying $\mathcal{N}$ with

$$h(x_c) = 1 - f(x_c), \tag{33}$$

where $x_c = \mathrm{Ra}/\mathrm{Ra}_c$. The function $h(x_c)$ obeys the properties $h(x_c \to 0) \to 0$ and $h(x_c \to \infty) \to 1 - 1/x_c \to 1$, which ensures that $\mathrm{Nu} \to 1$ in the purely diffusive equilibrium. The crossover function connects these two states smoothly, so that at $\mathrm{Ra} = \mathrm{Ra}_c$ we have $h(1) \approx 0.16$ instead of an abrupt jump to zero. Since we cannot determine $\mathcal{N}$ directly, we transform $\mathrm{Nu} - 1 = h(x_c)\mathcal{N}$ into $(\mathrm{Nu}-1)/h(x_c) = \mathcal{N}$, and in the Re-independent equation we replace $\mathrm{Nu} - 1$ by $(\mathrm{Nu}-1)/h(x_c)$. This gives the same result of $\mathrm{Nu} = 1$ in the nonconvective regime once the equation is solved for Nu by numerical methods. Thus the final model equations are (32) and

$$\frac{(\mathrm{Nu}-1)\mathrm{Ra}}{\zeta^2\mathrm{Pr}^2 h(\mathrm{Ra}/\mathrm{Ra}_c)} = c_1\zeta g\left(\frac{\zeta}{\mathrm{Re}^*}\right) + c_2\mathrm{Ha} + c_3\mathrm{Ha}^2 + c_4\mathrm{Ha}^3, \tag{34}$$

with

$$\zeta = \frac{\left(\sqrt{c_6^2 + \frac{4c_5(\mathrm{Nu}-1)}{h(\mathrm{Ra}/\mathrm{Ra}_c)}} - c_6\right)^2}{4c_5^2\mathrm{Pr} f\left(\frac{2\,\mathrm{Nu}}{\mathrm{Ha}}\right)}. \tag{35}$$

Now (34) can be used to determine the seven model parameters Re^* and c_1–c_6 by fitting the equation to a data set (Nu, Ra, Ha, Pr). However, examining (34) shows that it is invariant for the following transformations:

$$c_1 \to \alpha^6 c_1, \quad c_2 \to \alpha^4 c_2, \quad c_3 \to \alpha^4 c_3,$$
$$c_4 \to \alpha^4 c_4, \quad c_5 \to \alpha^2 c_5, \quad c_6 \to \alpha c_6, \quad \mathrm{Re}^* \to \mathrm{Re}^*/\alpha^2$$

for any $\alpha \in \mathbb{R}$. This means that the optimal values for the model parameters are ambiguous. To fix this ambiguity, we need at least one data point (Re, Nu, Ra, Ha, Pr), which includes the Reynolds number. Then (32) can be used to calculate c_6 as a function of c_5:

$$c_6 = \frac{\mathrm{Nu}-1}{\sqrt{\mathrm{Re}\,\mathrm{Pr} f\left(\frac{2\,\mathrm{Nu}}{\mathrm{Ha}}\right)}} - c_5\sqrt{\mathrm{Re}\,\mathrm{Pr} f\left(\frac{2\,\mathrm{Nu}}{\mathrm{Ha}}\right)}. \tag{36}$$

With this step, the optimal values of all remaining six model parameters Re^* and c_1–c_5 are unique. It is absolutely clear that six parameters, which have to be adjusted, is still a large number. Nevertheless, one has to keep in mind that the number of free parameters has already been reduced significantly. We are not aware of any publications that report magnetoconvection data sets including Re. Therefore, we are using our own numerical simulations to determine data points (Re, Nu, Ra, Ha, Pr) for evaluating (36).

IV. RESULTS

Our numerical simulations are used to evaluate (36). After substituting (36) into (34), the resulting equation is fitted to the experimental data of Cioni *et al.* [23] in terms of Re^* and c_1–c_5, utilizing the Levenberg-Marquardt method [27]. The experimental data have been obtained for convection in liquid mercury at a Prandtl number of $\mathrm{Pr} = 0.025$. Our DNS are conducted at the same Prandtl number. With the known optimal model parameters, we can calculate Nu by solving (34) numerically for given Ra, Ha, and Pr, and subsequently we obtain Re from (32). The optimal model parameters are $\mathrm{Re}^* = 56\,000$, $c_1 = 0.053$, $c_2 = -2.4$, $c_3 = 0.014$, $c_4 = -3.7 \times 10^{-6}$, and $c_5 = 0.0038$. From (36) we get $c_6 = 0.47$. The Ra-Ha phase diagrams for Nu and Re calculated with these parameter values for $\mathrm{Pr} = 0.025$ are shown in Fig. 2. The top panel of the figure shows the magnitude of the Nusselt number as a function of Ha and Ra. The bottom figure displays the Reynolds number depending on both parameters. Also added

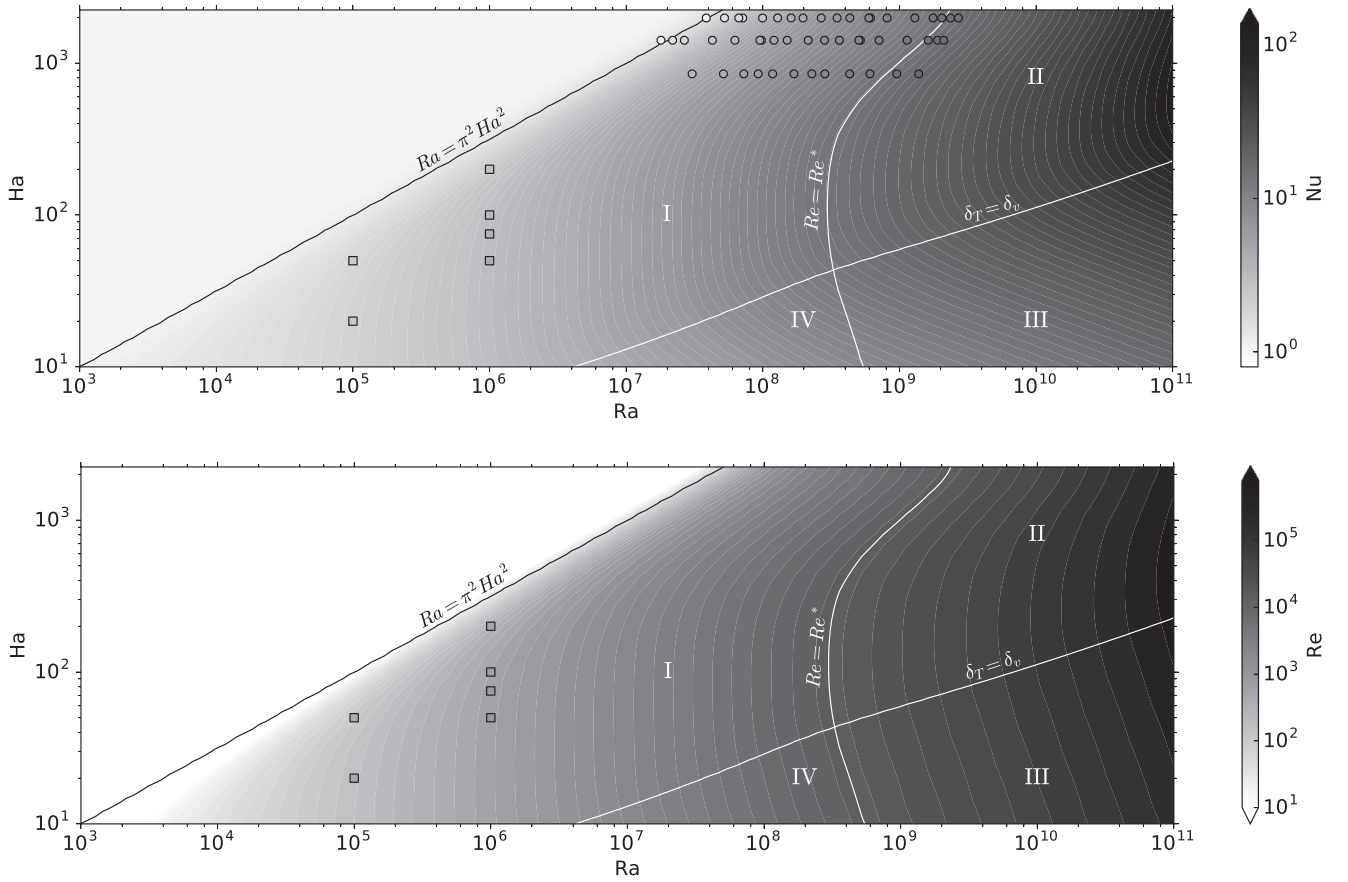

FIG. 2. Phase diagrams of (a) Nu and (b) Re on the Ra-Ha plane for Pr = 0.025. The symbols represent the data of our numerical simulations (squares) and the experiments by Cioni *et al.* [23] (circles) used for fitting the model parameters. The lines in the diagrams mark the position of the crossovers introduced in the model: Below $\delta_T = \delta_v$, the scaling of the thermal BL dissipation changes, $\mathrm{Re} = \mathrm{Re}^*$ marks the transition range from a weakly nonlinear to a fully turbulent bulk flow, and $\mathrm{Ra} = \pi^2 \mathrm{Ha}^2$ indicates the onset of convection. Regimes I–IV are marked as described in the text.

are the experimental and DNS data. In Fig. 2, we also display the Chandrasekhar limit above which Nu = 1 and Re = 0.

Furthermore, the line is displayed for which $\delta_v = \delta_T$. Above this line, the Hartmann layer thickness will be smaller than the thermal boundary layer thickness. This characteristic line is crossed by a second line that shows $\mathrm{Re} = \mathrm{Re}^*$. As mentioned already in Sec. III [see Eq. (18)], on the left side of this line the convection flow is not fully developed turbulent, but it is in a weakly nonlinear and time-dependent convection regime. All data that are to the right of this line can be considered as fully turbulent convection data. It can be seen that only a few data points of [23] cross this threshold. These two lines, therefore, split the parameter space into four subregions:

Region I: weakly nonlinear flow and strong magnetic field.

Region II: fully developed turbulent flow and strong magnetic field.

Region III: fully developed turbulent flow and weaker magnetic field.

Region IV: weakly nonlinear flow and weaker magnetic field.

A few points about the quality of the fit should be addressed now. First, we mention that the size of the error bars of all fit coefficients (except c_6) is of the order of 100%. In the case of the coefficient c_2, this error level is even exceeded (see also the following paragraphs). This is caused by the sparse record of data points. As can be seen in the figure, the data of Cioni *et al.* [23] are collected for three different Hartmann numbers

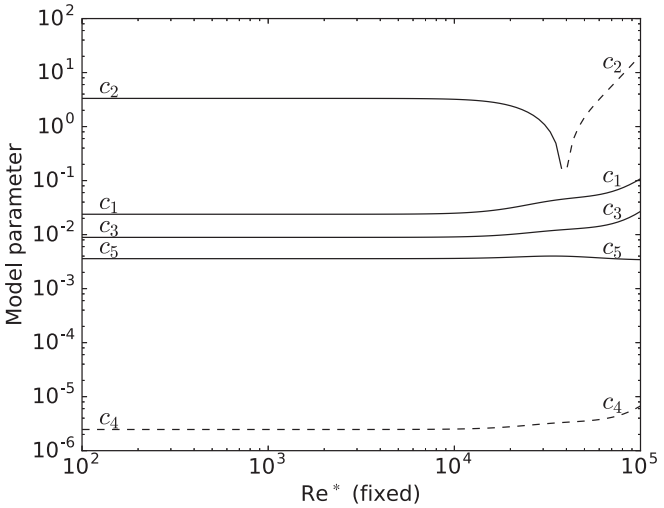

FIG. 3. Dependence of the coefficients c_1–c_5 when fixing the sixth coefficient Re^*. Negative values of c_2 and c_4 are indicated by a dashed line.

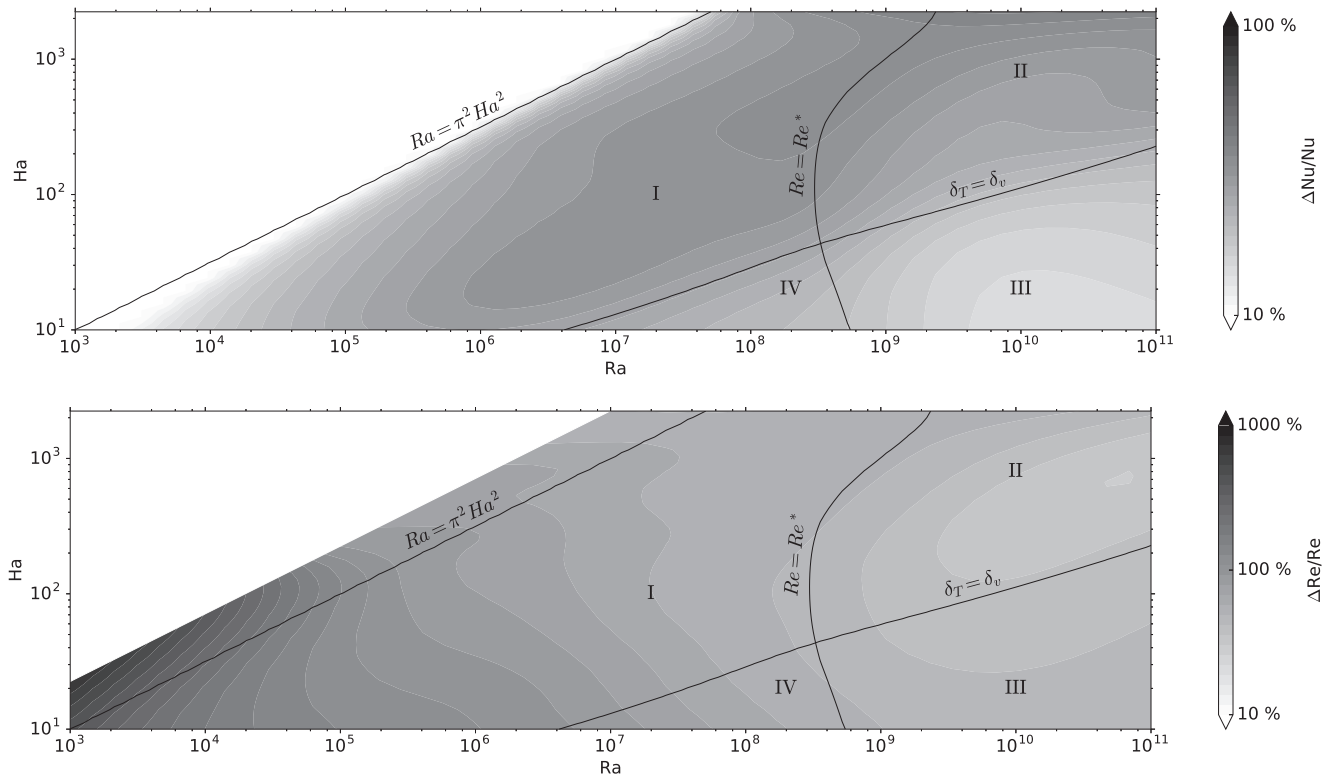

FIG. 4. Uncertainty of (a) Nusselt and (b) Reynolds number results in parameter space. The relative errors, ΔNu/Nu and ΔRe/Re, are shown in a logarithmic scale. The data are obtained by varying the fit coefficients $c_1, \ldots, c_5$ and Re^* independently of each other within their error bars. Regimes I–IV and their borders are marked as in Fig. 2, and the purely conductive regime has been masked.

that cover a small range. Also, these data reach only to the beginning of regime II. Regimes III and IV do not contain any data points. Stevens *et al.* [28] demonstrated in their recent update of GL theory that the uncertainties in the coefficients can be significantly reduced when the data cover a wide range of parameters. Furthermore, these three Hartmann numbers are much larger than those from our DNS. The additional data by Burr and Müller [24] or by Aurnou and Olson [25] have been conducted close to the onset regime of convection. Their experimental data are thus in the weakly nonlinear rather than in the fully turbulent range, and they will not be used for our study.

Secondly, it is observed that two fit coefficients, c_2 and c_4, are negative. Although $c_4 \sim 10^{-6}$ and thus is practically zero, the corresponding term in (34) can give a non-negligible contribution to the scaling due to Ha^3. The coefficient c_2 with the biggest error bar needs further consideration. Figure 3 displays the five coefficients in dependence of a fixed Re^*. To get this figure, we repeated the fits at each fixed value of the crossover Reynolds number. It is seen that the results for c_1–c_5 are nearly insensitive for $\mathrm{Re}^* \lesssim 2 \times 10^4$. Beyond this value, the coefficient c_2 changes sign, which is indicated by a dashed line in the plot. The eventual value of c_2 falls into a range in which small variations of Re^* cause large changes of c_2 (including sign changes).

The magnitude of $\mathrm{Re}^* \sim 5 \times 10^4$ in our fit corresponds to a Rayleigh number of $\mathrm{Ra} \sim 10^9$. This estimate follows from recent numerical studies in liquid-metal convection without magnetic field [29]. It falls thus consistently in the range for which convection develops into the fully developed turbulent regime, which is also known as the hard convective turbulence regime [30]. At the moment, we can only speculate that the inclusion of more data could lower the value of Re^*, as is expected in low-Pr convection (see, e.g., [31,32]).

Thirdly, in order to quantify the impact of the error bars of the fit coefficients on Nu(Ha, Ra) and Re(Ha, Ra), we proceeded as follows. The six coefficients $c_1, \ldots, c_5$ and Re^* were chosen randomly and statistically independently within their error bars. With these 6-tuples, the parameter dependence Nu(Ha, Ra) and Re(Ha, Ra) is reconstructed for 118 different cases. The superposition of these individual realizations results in a relative error around the original value in Fig. 2. The magnitudes of the relative error of both the Nusselt and Reynolds numbers are plotted in logarithmic units in Fig. 4. The relative error of Nu is highest along the border between regime I and II, but it does not exceed 40%. On the other hand, the relative uncertainty of Re rises for smaller Ra and reaches more than 100% for Ra below 10^6.

V. SUMMARY

We have presented an extension of the scaling theory of Grossmann and Lohse [8,9] to a convection layer in the presence of a vertical magnetic field. The discussion is restricted to magnetoconvection at low Prandtl and magnetic Prandtl numbers. In this regime, the quasistatic approximation is applied that allows a significant reduction of the number of free parameters in the flow at hand and thus an application of the ideas of GL theory. Below the Chandrasekhar limit, four different convection regimes are identified. On the one

hand, they follow from the ratio of the Hartmann and thermal boundary layer thicknesses. On the other hand, the regions result from the critical Reynolds number Re^*, beyond which the convection flow is assumed to be fully turbulent.

In contrast to standard Rayleigh-Bénard convection, the database is very small. In fact, there is only one dataset from Cioni and co-workers, which can be used to fit the free parameters. The remaining data [24,25] fall into a completely different section of the parameter plane. In particular, they remain close to the Chandrasekhar limit and cannot be used for turbulent magnetoconvection. This limits the predictive capabilities of our scaling results and calls for additional experimental and numerical data, which are planed in the near future.

ACKNOWLEDGMENTS

T.Z. and W.L. are supported by the Research Training Group "Lorentz Force Velocimetry and Lorentz Force Eddy Current Testing", which is funded by the Deutsche Forschungsgemeinschaft under Grant No. GRK 1567. W.L. is additionally supported by a Fellowship of the China Scholarship Council. The work of D.K. is supported by the Helmholtz Research Alliance "Liquid Metal Technologies", which is funded by the Helmholtz Association. We thank Jonathan Aurnou, Detlef Lohse, and in particular Bruno Eckhardt for helpful discussions.

APPENDIX: HARTMANN LAYER

The Hartmann problem [33] describes an isothermal pressure-driven plane Poiseuille channel flow subject to a vertical homogeneous magnetic field (see also [20]). The starting point is Eq. (4) for $T = T_0$. One seeks a steady solution $u_x(z)$ in the quasistatic regime. This results in the inhomogeneous differential equation

$$\rho_0 \nu \frac{d^2 u_x(z)}{dz^2} - \sigma B_0^2 u_x(z) = -G, \tag{A1}$$

with $\partial p/\partial x = -G = \text{const}$. The Hartmann layer thickness (17) arises as the characteristic length scale in the problem, and it is given by

$$\delta_v = \sqrt{\frac{\rho_0 \nu}{\sigma B_0^2}} = \frac{H}{\mathrm{Ha}}. \tag{A2}$$

[1] L. P. Kadanoff, Phys. Today **54**(8), 34 (2001).
[2] G. Ahlers, S. Grossmann, and D. Lohse, Rev. Mod. Phys. **81**, 503 (2009).
[3] F. Chillà and J. Schumacher, Eur. Phys. J. E **35**, 58 (2012).
[4] W. V. R. Malkus, Proc. R. Soc. London, Ser. A **225**, 185 (1954).
[5] W. V. R. Malkus, Proc. R. Soc. London, Ser. A **225**, 196 (1954).
[6] B. I. Shraiman and E. D. Siggia, Phys. Rev. A **42**, 3650 (1990).
[7] E. D. Siggia, Annu. Rev. Fluid Mech. **26**, 137 (1994).
[8] S. Grossmann and D. Lohse, J. Fluid Mech. **407**, 27 (2000).
[9] S. Grossmann and D. Lohse, Phys. Rev. Lett. **86**, 3316 (2001).
[10] Y. Yang, E. P. van der Poel, R. Ostilla-Monico, C. Sun, R. Verzicco, S. Grossmann, and D. Lohse, J. Fluid Mech. **768**, 476 (2015).
[11] O. Shishkina, S. Grossmann, and D. Lohse, Geophys. Res. Lett. **43**, 1219 (2016).
[12] N. O. Weiss and M. R. E. Procter, *Magnetoconvection* (Cambridge University Press, Cambridge, 2014).
[13] M. Rempel and R. Schlichenmaier, Living Rev. Sol. Phys. **8**, 60 (2011).
[14] A. J. Castro-Tirado *et al.*, Nature (London) **455**, 506 (2008).
[15] R. W. Series and D. T. J. Hurle, J. Cryst. Growth **113**, 305 (1991).
[16] N. Shevchenko, O. Roshchupkina, O. Sokolova, and S. Eckert, J. Cryst. Growth **417**, 1 (2015).
[17] T. Ihli *et al.*, Fusion Eng. Design **83**, 912 (2008).
[18] S. Chandrasekhar, *Hydrodynamic and Hydromagnetic Stability* (Dover, New York, 1961).
[19] Y. Tasaka, K. Igaki, T. Yanagisawa, T. Vogt, T. Zuerner, and S. Eckert, Phys. Rev. E **93**, 043109 (2016).
[20] P. A. Davidson, *An Introduction to Magnetohydrodynamics* (Cambridge University Press, Cambridge, 2008).
[21] S. Chakraborty, Physica D **237**, 3233 (2008).
[22] R. M. Kulsrud, Annu. Rev. Astron. Astrophys. **37**, 37 (1999).
[23] S. Cioni, S. Chaumat, and J. Sommeria, Phys. Rev. E **62**, R4520 (2000).
[24] U. Burr and U. Müller, Phys. Fluids **13**, 3247 (2001).
[25] J. M. Aurnou and P. L. Olson, J. Fluid Mech. **430**, 283 (2001).
[26] D. Krasnov, O. Zikanov, and T. Boeck, Comput. Fluids **50**, 46 (2011).
[27] J. J. Moré, *The Levenberg-Marquardt Algorithm: Implementation and Theory* (Springer, Berlin, 1978).
[28] R. J. A. M. Stevens, E. P. van der Poel, S. Grossmann, and D. Lohse, J. Fluid Mech. **730**, 295 (2013).
[29] J. D. Scheel and J. Schumacher, J. Fluid Mech. **802**, 147 (2016).
[30] B. Castaing, G. Gunaratne, F. Heslot, L. Kadanoff, A. Libchaber, S. Thomae, X. Z. Wu, S. Zaleski, and G. Zanetti, J. Fluid Mech. **204**, 1 (1989).
[31] T. Mashiko, Y. Tsuji, T. Mizuno, and M. Sano, Phys. Rev. E **69**, 036306 (2004).
[32] J. Schumacher, P. Götzfried, and J. D. Scheel, Proc. Natl. Acad. Sci. (USA) **112**, 9530 (2015).
[33] J. Hartmann, K. Dan. Vidensk. Selsk., Mat.-Fys. Medd. **15**, 1 (1937).